Complete Flow for PCB Design Consideration and Power/Signal Integrity Analysis Based on Broadband Model of Parasitic Elements

International Journal of Circuit Theory and Applications

WILEY

BRIEF REPORT OPEN ACCESS

Complete Flow for PCB Design Consideration and Power/Signal Integrity Analysis Based on Broadband Model of Parasitic Elements

Silvia Simone[1] | Fabio Pareschi[1] | Davide Lena[2] | Gianluca Setti[3]

[1]DET, Politecnico di Torino, Torino, Italy | [2]STMicroelectronics S.R.L., Torino, Italy | [3]CEMSE, King Abdullah University of Science and Technology (KAUST), Thuwal, Saudi Arabia

Correspondence: Silvia Simone (silvia_simone@polito.it)

Received: 2 September 2025 | **Revised:** 30 October 2025 | **Accepted:** 5 December 2025

Keywords: broadband model | EM simulation | parasitic components | power integrity | signal integrity

ABSTRACT

A new implementation of a broadband model for the generation of an accurate time-domain description of parasitic elements from frequency-domain electromagnetic (EM) simulator results is here proposed. The model is designed to work simultaneously at low and high frequencies, bypassing EM simulators limitations. A further investigation on the appropriate reference impedance selection during the transformation of data from frequency to time-domain is conducted. The resulting model is validated against measurement and applied to a practical design case, illustrating the operational steps of the novel workflow.

1 | Introduction

Considering the impact of parasitic elements in the early stages of the development of modern electronic systems is essential to ensure reliability and performance. Taking them into account only after the design stage, in fact, may result in not meeting certain requirements or performance specifications, making necessary the full revision of the project. Given this, the use of EM simulators in the parasitic identification becomes an essential step of the design process, as it represents the only way to avoid additional iterations in the project development that would increase the time-to-market and the overall costs.

The 3D tools are employed to handle structures with arbitrary geometry and capture electromagnetic (EM) coupling in all spatial directions [1]. Based on Maxwell's equations, these solvers can be classified as quasi-static or full-wave depending on the method and approximation of the adopted solution. The first ones consider the quasi-static approximation of Maxwell's equations, relying on the assumption that the time variation of EM fields is sufficiently slow, such that wave propagation effects can be neglected [2–4]. Their solution is valid under the condition that the wavelength of the EM wave λ is very large compared to the size d of the system: $d < \lambda/10$ [5]. Full-wave solvers are instead based on the complete set of Maxwell's equations and accurately capture high-frequency effects. They are affected by the low-frequency breakdown problem, and the solutions become less accurate when the frequency decreases [6–8]. To address this issue, major EM simulation tools provide two distinct options, allowing EM analysis to be performed with the most appropriate solver for the frequency range of interest. In particular, ANSYS provides two distinct tools: HFSS for full-wave high-frequency simulations and Q3D extractor for quasi-static analysis. Similarly, Altair offers Feko and Flux, which correspond, respectively, to the aforementioned categories. COMSOL multiphysics allows the use of a dedicated module for low-frequency simulations, the AC/DC one, while CST studio suite provides the option to select the low-frequency solver for quasi-static problem.

Alternatively, other studies have investigated computational strategies based on different formulations of Maxwell's

equations to overcome the low-frequency breakdown problem and preserve numerical stability [9]. However, these methods cannot be directly implemented in standard commercial software because they require explicit access to the system matrices obtained from the discretized equations, which are not available to the user. As a consequence, achieving accuracy in a broadband range of frequency, from DC to GHz simultaneously, is particularly challenging. This is, however, extremely important for many applications. An example is power integrity analysis, where a reliable and stable power delivery network must be maintained across a wide frequency spectrum, and impedance across frequencies must be minimized to ensure low voltage fluctuations. Another example is signal integrity analysis, where an accurate modeling of printed circuit board (PCB) traces, connectors, vias, and so on, is essential to take into account effects such as reflection, crosstalk, timing jitter that are highly frequency dependent, thus enabling precise timing analysis.

The aim of this brief paper is to propose a clearly defined process for developing an accurate model across a wide frequency range, while at the same time ensuring consistency after time-domain conversion. To the best of our knowledge, this has not been fully addressed in the literature.

The paper is organized as follows. Section 2 provides a detailed comparison with existing studies along with an explanation of the proposed workflow. Then, in Section 3, the methodology to perform the measurements and compare them with the results of EM tools is explained. In Section 4, the workflow is detailed explaining the procedure for generating the broadband model and the conversion of the data from frequency to time-domain. In Section 5, the results are outlined and an application of the proposed model is compared to measurements data, finally the conclusions are drawn.

2 | Simulation Workflow and Design Procedure

As introduced, parasitic elements plays a critical role in the design process and must be carefully considered. To address this challenge, several studies have proposed high-level design approaches.

In Table 1, a comparison with the current state of the art is presented. The various approaches are analyzed, highlighting the aspects in which these methodologies exhibit limitations.

Thus, a more general and rigorous procedure is required to ensure simulation results are accurate and meaningful within the context of the specific application under investigation. Considering the need to employ commercially available EM solvers for a practical and computationally feasible analysis, it thus becomes evident that, given the inherent validity constraints of each solver, adopting a multitool strategy is essential to obtain an accurate model over a wide frequency range. The results obtained from quasi-static and full-wave solvers must be combined to construct a unified description valid over the entire frequency range of interest. It can subsequently be transformed into a time-domain model, to perform transient cosimulation with circuit level components, requiring that the resulting netlist accurately preserves the original frequency-domain behavior to ensure reliable results.

The novel workflow can therefore be defined as schematized in Figure 1.

3 | Evaluation Method of PCB Parasitic Elements With Simulations and Measurements

To perform a comprehensive and detailed analysis of the parasitic elements, a customized two-layer PCB has been developed, with a substrate made of FR4 and a thickness of 1.6 mm, a copper

TABLE 1 | Comparison with existing solutions.

Methodology	Reference	Approach	Considerations
QS-FW	[10–12].	Comparison of the results with different models obtained with quasi-static and full-wave simulators.	Two separate models are needed, depending on the frequency range of interest. Each model is accurate within its validity region, but a consistent time-domain analysis can not be performed without a unified description.
EM-simulation	[13].	Step of EM simulation: creation of the physical model, setup of simulation, postprocessing of results.	Preliminary approach, no broadband frequency considerations. By obtaining only S-parameters, transient analysis can not always be executed or accurately resolved using SPICE-based tools.
Cosimulation	[13–16].	Example of the applications of the model of parasitic elements for design considerations.	Details on how to obtain a time-domain model are not provided. If considerations on reference impedance and passivity are not addressed the resulting model can be entirely inaccurate or lead to unstable behavior.
EM model workflow	Proposed	Procedure to obtain accurate broadband time-domain model starting from EM simulations to cosimulations.	Single broadband model with controlled accuracy. Based on the same EM simulations as previous approaches but adding a reprocessing of results. It enables the possibility of conducting precise time-domain analysis.

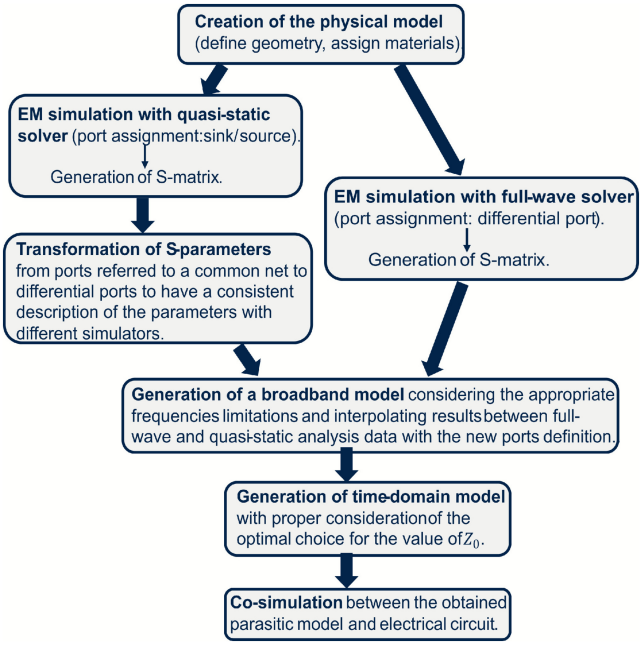

FIGURE 1 | Proposed flow for the generation of an accurate time-domain model of parasitic suitable for SPICE-like circuit simulation.

trace with a height of 0.035 mm, width of 1.8 mm, and a length of 770 mm; at the ends of the trace, vias are employed to provide a connection to the underlying ground plane. In order to correctly measure the impedance of the trace, a shunt through measurement is performed, which is the standard method capable of capturing very low impedance values up to very high frequencies [17, 18]. With this methodology, S-parameters are measured using vector network analyzer (VNA), in particular Bode 100 that works up to frequencies equal to 40 MHz and Rigol RSA 3030N, used for measurements at higher frequencies, starting from MHz range up to 3 GHz. However, the ground connection of the VNA creates an unwanted alternative path for the current signal, resulting in a measurement error [19]. To address the issue associated with ground loop problems, a common mode transformer is inserted to block the common mode current. The described test configuration is illustrated in Figure 2.

For the two-port network, the S-parameter measurements can be translated into an impedance measurement as follows [20]:

$$S_{21} = \frac{2V_2}{V_1 + I_1 Z_0} = \frac{2Z}{2Z + Z_0}, \qquad Z = \frac{Z_0 S_{21}}{2(1 - S_{21})}, \tag{1}$$

where $V_{1,2}$ represent the voltages across the two ports and I_1 is the current entering port one. Z_0 corresponds to the reference impedance, while Z is the impedance of the device under test. The parasitic resistance and inductance are derived by extracting, respectively, the real (Re) and imaginary (Im) part of the obtained impedance:

$$R = Re(Z), \qquad L = Im\left(\frac{Z}{2\pi f}\right). \tag{2}$$

For the comparison with simulation results, both a quasi-static tool, Q3D, and a full-wave one, HFSS, from Ansys environment, were employed to achieve accurate solutions across different operating

FIGURE 2 | Measurement setup with Bode 100 (and Rigol RSA 3030N) as VNA, J2102B Common Mode Transformer, two-port probe P2102A and PCB layout.

conditions. The first one was used under the low-frequency approximation previously explained, whereas the latter was adopted to accurately model the EM behavior at higher frequencies.

With the Ansys quasi-static simulator, for each conductor, a sink and multiple sources can be defined. To obtain the self-inductance/resistance values between the sink and each source, the sink of the interested net must be closed to the reference ground terminal, and in this configuration, the Z-matrix can be computed to subsequently derive the values [21]. With the full-wave simulator instead, it is not possible to obtain partial parasitic inductance and resistance between two specific points (i.e., sink and source in Q3D), but only loop values can be computed; thus, loop values of parasitic components are obtained starting from the matrix of Y-parameters as follows:

$$R = Re\left(\frac{1}{Y_{i,i}}\right), \qquad L = Im\left(\frac{1}{Y_{i,i} 2\pi f}\right). \tag{3}$$

In this condition, the parasitic values of inductance and resistance of the described PCB are measured and simulated.

As illustrated in Figure 3, the results of the low frequencies simulation with Q3D align perfectly with the experimental measurements with Bode 100. Instead, when the frequency is higher than $v_p/(10d) \approx 20$ MHz, where $v_p = c/\sqrt{\epsilon_r}$ is the propagation velocity in a medium, with c equal to the speed of light and ϵ_r is the relative dielectric constant of FR4, the quasi-static limit is exceeded and the measurements performed with the Rigol VNA closely match the HFSS results, which, by contrast, at low frequencies exhibit a relative error between 20% and 40% for inductance and resistance values.

4 | Generation of Accurate Time-Domain Model of Parasitic Element

4.1 | Broadband Model Implementation

A second PCB, with the same material definition, trace width, and thickness as the previous one, is then realized to consider a n-port device (Figure 4a), where, in this case, n is equal to 7. As in

the previous case, for the EM analysis, differential ports are set in HFSS, while in Q3D, a sink or a source is located where in the full-wave solver, the positive and negative terminal of the differential port is present (Figure 4b). Therefore, in HFSS, an S-matrix with n differential ports is obtained, while the port configuration in Q3D leads into a $2n$ ports S-matrix referred to a common net. To transform the Q3D matrix in the same format as HFSS, the Keysight tool ADS is used, and the new S-parameters are extracted forcing the reference net of the terminal to the corresponding sink or source present in the Q3D EM simulation (Figure 4c). In this way, a model directly comparable with HFSS is obtained, the S-matrices from the two different tools are now described in the same format, and it is possible to generate a broadband model valid from DC to GHz, using a hybrid approach.

The matrix of S-parameters extracted with Q3D is employed for the low-frequency region, while the matrix extracted with HFSS is adopted for the high-frequency region. In order to correctly combine the two systems, Q3D data are considered starting one decade before the quasi-static limit equal to $v_p/(10d)$ to ensure the validity of low-frequency data. Beyond this limit, we can also ensure that HFSS data are correct since the low-frequency breakdown problem is no longer present. The intervals under consideration are highlighted in Figure 3. In the remaining decade of frequencies between these two systems, spline interpolation is applied to provide a smooth and precise transition between the values, ensuring that the connection of the two systems is continuous and consistent. This procedure enables the derivation of a model composed of a single S-matrix that accurately characterizes the system behavior across the entire frequency range.

4.2 | Time-Domain Conversion

The last step required to enable time-domain simulation is the transformation of the model from frequency to time-domain. This final part of the workflow ensures that the system can be accurately integrated into circuit simulators that operate in time-domain, such as SPICE-based tools. The S-parameters data must then be verified for passivity, as nonpassive models can lead to instability in time-domain simulations. Additionally, causality must be preserved, which is necessary to maintain its physical meaning. Moreover, it is essential that the transformation guarantees a high level of accuracy of the system behavior; otherwise, the reliability and performance of the model are compromised.

To this end, simulators capable of converting S-parameters into their time-domain representation must be employed. In order to achieve an accurate conversion, let us make some considerations. According to [22] the reflection coefficient can be written as follows:

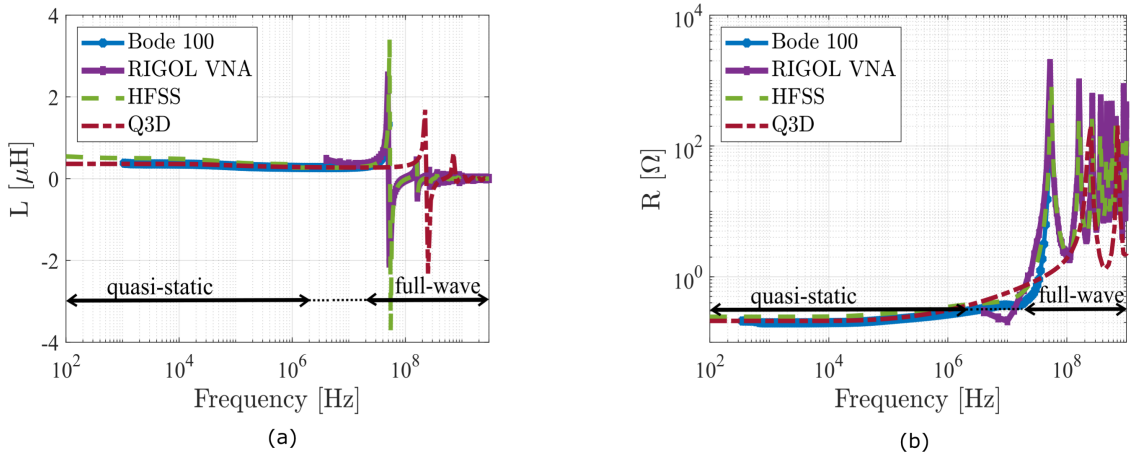

FIGURE 3 | Comparison between parasitic (a) inductance and (b) resistance of the described PCB, obtained with measurement using Bode 100 and Rigol RSA 3030N VNA and with simulation employing Q3D and HFSS.

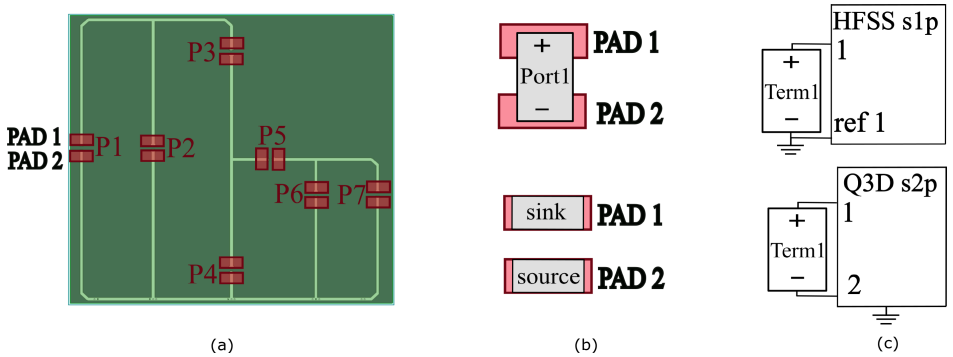

FIGURE 4 | (a) N-ports PCB, and different port configuration, considering one port as example, between (b) HFSS and Q3D for EM analysis and (c) ADS for the translation in the same format.

$$S_{ii} = \frac{Z_{\text{in}}^{(i)} - Z_0}{Z_{\text{in}}^{(i)} + Z_0}, \tag{4}$$

with $Z_{\text{in}}^{(i)}$ equal to the input impedance at port i looking into the matching section.

In Figure 5a, the behavior of S_{ii} in (4) is illustrated by fixing the reference impedance to 50Ω while varying both the real and imaginary components of Z_{in}. It is evident that the behavior of the reflection coefficient is strongly influenced by variations in the real part of Z_{in}. Specifically, when that quantity becomes much larger than the value of Z_0, as highlighted in the region labeled as "A", the magnitude of the reflection coefficient consistently converges towards 1. As a result, values of the real part of $Z_{\text{in}}^{(i)}$ very different from each other lead to very similar values of the magnitude of S_{ii}. Instead, when the real part of $Z_{\text{in}}^{(i)}$ approaches the reference impedance value, as depicted in the second region "B", a bending occurs in the curve representing $|S_{ii}|$, meanwhile the increase of its imaginary part determines a slight increase in the reflection coefficient amplitude. Therefore, the range of the represented S-parameter expands significantly. In a different point of view, the precision required during the fitting process strongly depends on the region in which the analysis is performed. Let us estimate the resolution associated with the fitting process by computing the difference between the minimum and the maximum quantity of the absolute value of the reflection coefficient in each region as follows:

$$\delta_{S_{ii}} = (|S_{ii}|_{\max} - |S_{ii}|_{\min}) \cdot \epsilon_{\%}. \tag{5}$$

A tolerance factor ϵ, expressed as a percentage of this range, is applied to reflect the desired level of precision required for the model. Considering $\epsilon_{\%} = 0.01$ and assuming both regions cover the same number of decades (i.e., region "A": $5 \cdot 10^{-5}$–$5 \cdot 10^{-1}\Omega$ and region "B": $5 \cdot 10^{-1}$-$5 \cdot 10^{3}\Omega$), we can compute $\delta_{S_{ii}}$ that is the value we require to set in the fitting process as absolute tolerance. In the first region, it is approximately equal to $1.8 \cdot 10^{-4}$, instead in the second region $\delta_{S_{ii}} \approx 1.8 \cdot 10^{-2}$. It is clear that this second option substantially reduces the required tolerance error, maintaining the same precision of the fitted parameters. Thus, the optimal value of Z_0 to be selected during the creation of the model is such that it closely approaches the real part of Z_{in}. Relaxing the tool error tolerance during the fitting process is not only beneficial in terms of numerical simulation but also results in a less complex time-domain circuit netlist; conversely increased structural complexity may lead to a violation of the constraints on passivity and, in turn, could prevent the final simulation to converge. Additionally, the tool may not be able to achieve the level of precision required in the first region, degrading model accuracy.

A critical aspect is that the value of Z_{in} is influenced by the specific circuit configuration and the selected value of the reference impedance used to terminate the other ports during its computation. Consequently, once the S-parameters have been obtained from the EM simulation, it is possible to see Z_{in} variation for each port i, by changing the reference impedance of the derived S-parameters and then the input impedance value can be evaluated by inverting Equation (4). Taking as example the broadband S-parameters previously derived from the EM analysis of the n-port PCB, in Figure 5b, it is possible to observe the behavior of the real part of $Z_{\text{in}}^{(1)}$ varying the frequency and the reference impedance Z_0. Intersecting this curve with a plane equal to the reference impedance magnitude, that is the one used in the computation of the S-parameters from which $Z_{\text{in}}^{(1)}$ was derived, it is possible to identify a region outlined in red, before the system approaches its resonance frequency, in which it is more advantageous to select the reference impedance value during the fitting process, since the quantities corresponding to the real part of the input impedance and to Z_0 are close to each other.

In this way, it is possible to optimize the process and reduce the fitting error during the transformation of the parameters from frequency to time-domain. As a consequence, the procedure can be more effectively controlled, allowing for improved precision in the generation of the model and leading to an overall increase in the reliability of the results.

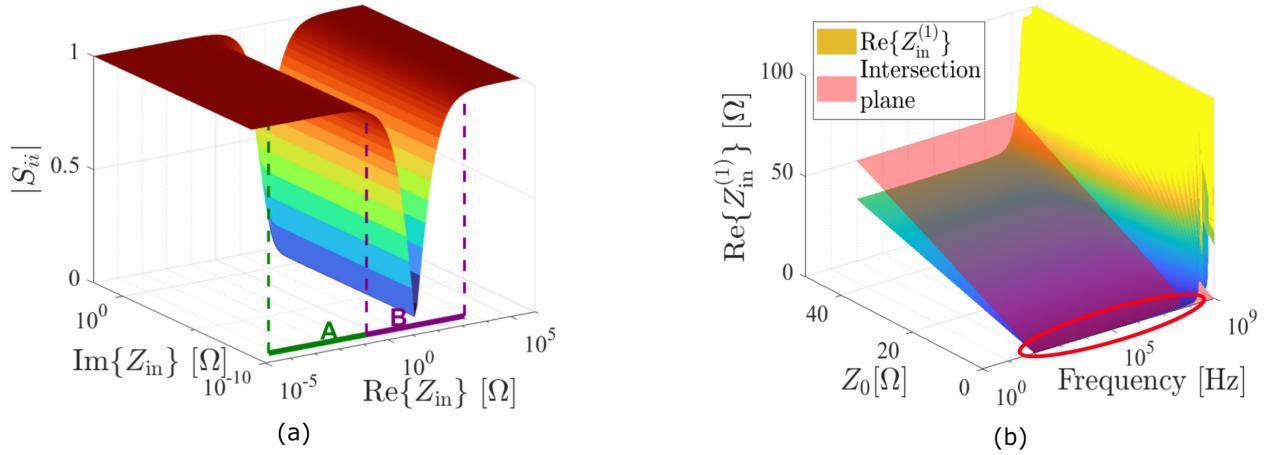

FIGURE 5 | (a) Magnitude of the variation of the reflection coefficient S_{ii} in (4) varying the real and imaginary part of Z_{in}, fixing the reference impedance Z_0 to 50Ω. (b) Variation of the real part of Z_{in} looking from port P1 (Figure 4a) as a function of frequency, varying Z_0, and intersection with plane $Z = Z_0$ highlighted in red.

5 | Model Comparison

Finally, a comparison between the derived model and measurements is carried out, with the aim of experimentally validating the model and verifying its accuracy. The two-port shunt through method is applied to the *n*-port PCB, placing the two-port probe across the positive and negative terminal of Port 1, considering the port definition in Figure 4a, short-circuiting Ports 2–4 and leaving the other ports open, to isolate and make a comparison of the parasitic contributions of the remaining portion of the loop. As in the case of the one-port PCB, the values of parasitic components are obtained starting from the measurement of the parameter S_{21}. For the simulation results, instead, the previously derived broadband model is adopted, and the software IdEM was employed for the generation of the time-domain netlist. As illustrated in Figure 6a, two netlists are derived using different reference impedances. For Z_0 equal to 50Ω, the magnitude of the represented S-parameter remains close to 1 below the resonance frequency. As a consequence, minor fitting variations in the S-parameter cause significant changes in the extracted parasitics value. Hence, higher tool accuracy is required, resulting in a more complex and nonpassive netlist. Conversely, the second netlist derived using an optimal value of Z_0 yields a passive and accurate model. Enforcing passivity, thus, becomes necessary for the first netlist, resulting, however, in a further reduction of accuracy, which can be observed in Figure 6b, where the parasitic inductance derived from the models is compared with measurements. The proposed technique, instead, accurately describes the behavior of parasitic components throughout the entire frequency range, with reliable results even after the transformation of S-matrix into time-domain, oppositely if Z_0 is not properly selected the accuracy degrades significantly.

A circuit suitable for time-domain simulator is consequently obtained and can be used in transient analyses by connecting it to the electrical components, allowing cosimulation between pure circuit schematic and EM simulation results.

Taking a practical case of study as an example, the equivalent circuit of the described *n*-port PCB can be employed for a detailed analysis of a DC/DC buck converter design. An analogous representation of the standalone converter is obtained, as can be seen in Figure 7, wherein now the broadband parasitic model is also included by attaching all electrical components to it, and the voltage at each port corresponds to the voltage across the connected component [23, 24]. It is now possible to carry out time-domain simulations to achieve a precise and optimized

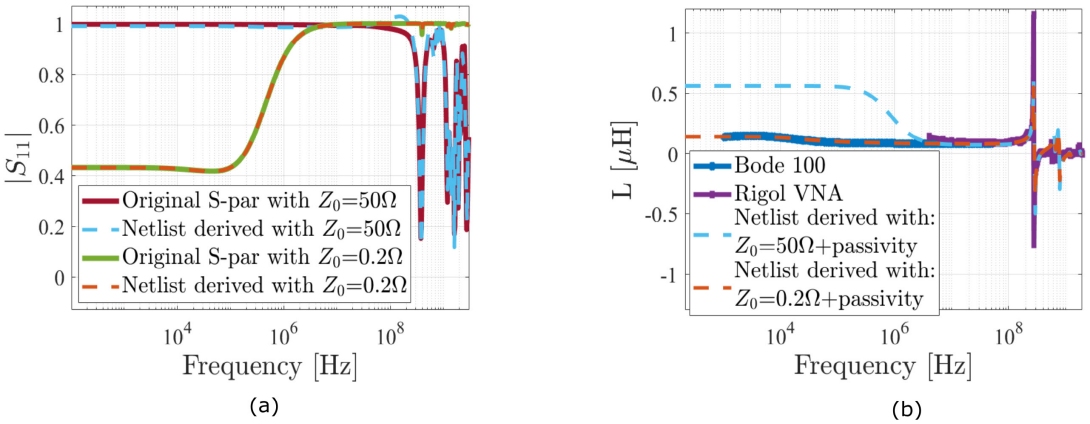

FIGURE 6 | (a) Comparison between original and derived S-parameters obtained from the time-domain netlist when Z_0 is equal to 50Ω and when it is close to Z_{in} seen from port P1 (Figure 4-a). (b) Comparison of the parasitic inductance estimated from measurements with Bode 100 and Rigol VNA and evaluated from the netlist with different Z_0, after ensuring passivity for both.

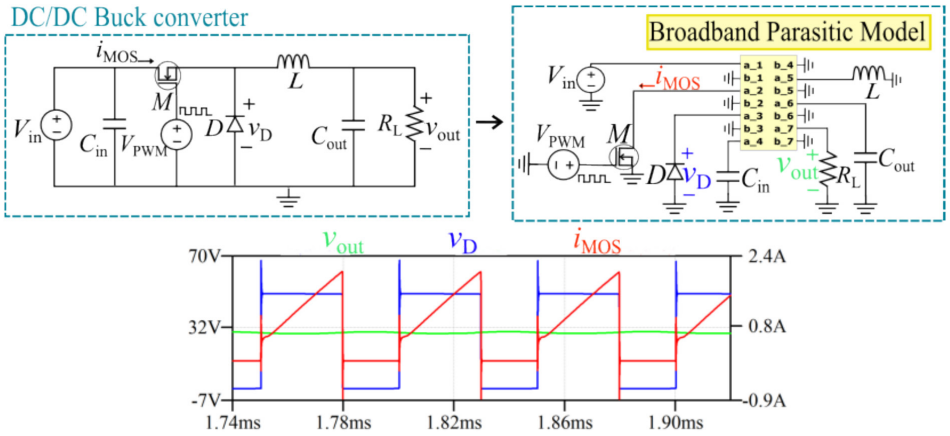

FIGURE 7 | Schematic of Buck converter and final equivalent model adding the netlist that reproduce EM simulation results. With this approach, cosimulation between pure electrical and parasitic components can be performed within a time-domain simulator; in this case, LTspice is employed and the main voltage and current waveforms of the converter are represented.

design of the device. Observing the voltage waveform across the inductor allows for the identification of the contribution of parasitic elements to voltage overshoots and high-frequency ringing, particularly during switching transients. In the same way, it is possible to analyze the voltage spikes that occur across critical components such as the transistors and the diode. This, in turn, enables a more accurate evaluation of whether these devices are operating within their respective safe operating areas (SOAs). Moreover, computing the voltage and current across the switching element with the inclusion of parasitic effects allows for a more realistic estimation of power losses, which are essential for thermal management and efficiency optimization. It is also possible to better evaluate the output voltage ripple for selecting appropriate output filtering components and ensuring stable operation of the converter. Finally, accurately modeling input current allows for an effective design of input electromagnetic interference (EMI) filter, ensuring compliance with electromagnetic compatibility (EMC) standards.

6 | Conclusions

Given the limitations of EM simulators, a quasi-static and full-wave tool are employed. The obtained S-parameters are combined to derive a broadband model that shows accuracy both at low and high frequencies. A detailed analysis of the choice of the reference impedance to be selected during the frequency-to-time domain transformation was conducted, deriving a broadband model suitable for time-domain simulation. Performing measurement on two different PCBs, the model is validated and then implemented to a practical case. The method is expected to remain well-controlled and effective even when applied to more complex structures, since it does not depend on geometry. Similar considerations on the transformation of the model from frequency to time-domain can also be applied to very high-frequency signals; however, further analysis to validate it under these conditions will be conducted.

Acknowledgments

This publication is part of the project PNRR-NGEU which has received funding from the MUR - DM 352 / 2022. Open access publishing facilitated by Politecnico di Torino, as part of the Wiley - CRUI-CARE agreement.

Conflicts of Interest

The authors declare no conflicts of interest.

Data Availability Statement

The data that support the findings of this study are available from the corresponding author upon reasonable request.

References

1. M. Bucolo, A. Buscarino, L. Fortuna, et al., "A Comparative Analysis of Computer-Aided Design Tools for Complex Power Electronics Systems," *Energies* 14, no. 22 (2021): 7729, https://doi.org/10.3390/en14227729.

2. J. D. Jackson, *Classical Electrodynamics*, 3rd ed. (Wiley, 1998).

3. S. E. Kruger, "*The Three Quasistatic Limits of the Maxwell Equations*" (2019). https://doi.org/10.48550/arXiv.1909.11264.

4. F. Rapetti and G. Rousseaux, "On Quasi-Static Models Hidden in Maxwell's Equations," *Applied Numerical Mathematics* 79 (2012): 92–106, https://doi.org/10.1016/j.apnum.2012.11.007.

5. *Q3D Extractor Help* (2025).

6. HFSS *Help* (2025).

7. J.-M. Jin, *The Finite Element Method in Electromagnetics*, 3rd ed. (Wiley-IEEE Press, 2014).

8. K. Umashankar and A. Taflove, *Computational Electromagnetics* (Artech House, 1993).

9. J. Zhu and D. Jiao, "A Rigorous Solution to the low-Frequency Breakdown in Full-Wave Finite-Element-Based Analysis of General Problems Involving Inhomogeneous Lossy Dielectrics and non-ideal Conductors," in *2011 IEEE MTT-S International Microwave Symposium* (IEEE, 2011), https://doi.org/10.1109/MWSYM.2011.5972841.

10. I. Kovacevic-Badstuebner, U. Grossner, and D. Popescu, "Tools for Broadband Electromagnetic Modeling of Power Semiconductor Packages and External Circuit Layouts," in *2020 32nd International Symposium on Power Semiconductor Devices and ICs (ISPSD)* (IEEE, 2020), 388–391, https://doi.org/10.1109/ISPSD46842.2020.9170161.

11. R. Malczyk, M. Bara, and H. Lu, "Estimation of SMPS Conducted Emission According to CISPR Standards," *Applied Sciences* 12, no. 3 (2022): 1458.

12. T. Moldaschl, S. Woetzel, R. Latella, M. Galvano, and A. Binder, "Comparison of the Parasitic Impedances From the Drainsource Path of Power Transistor Packages at up to 2 ghz," *Engineering Reports* 4, no. 5 (2022): e12489.

13. M. Bucolo, A. Buscarino, C. Famoso, et al., "Model Identification to Validate Printed Circuit Boards for Power Applications: A new Technique," *IEEE Access* 10 (2022), https://doi.org/10.1109/ACCESS.2022.3160449.

14. W. Belloumi, A. Breard, O. Hajji, C. Vollaire, and J. B. H. Slama, "Automatic PCB Layout Optimization of a DC-DC Converter Through Genetic Algorithm Regarding EMC Constraints," *IEEE Access* 9 (2021), https://doi.org/10.1109/ACCESS.2021.3124935.

15. L. Cui, Y. Zhang, R. Zhang, and Q. H. Liu, "A Modified Efficient KNN Method for Antenna Optimization and Design," *IEEE Transactions on Antennas and Propagation* 68, no. 10 (2020), https://doi.org/10.1109/TAP.2020.3001743.

16. R. Gordin, D. Goren, S. Shlafman, et al., "Design and Modeling Methodology of Vertical Interconnects for 3DI Applications," *IEEE Transactions on Components, Packaging and Manufacturing Technology* 1, no. 2 (2011), https://doi.org/10.1109/TCPMT.2010.2101751.

17. Keysight Technologies Application Note, "*Ultra-low impedance measurements using 2-port measurements*."

18. Picotest Application Note, "*Ultra-low Impedance (20 micro ohm) Measurement using 2-port Shunt-through*," (2018).

19. Picotest Application Note, "*The 2-port Shunt-through Measurement and the Iherent grGound Loop*," (2018).

20. "*Bode 100, bode 500 Vector Network Analyzer user Manual*," (2025).

21. S. Simone, F. Pareschi, D. Lena, and G. Setti, "Simulation Method for Quasi-Static Solver to Effectively Model Parasitic Components Between Package and PCB," in *2024 IEEE 33rd Conference on Electrical Performance of Electronic Packaging and Systems (EPEPS)* (IEEE, 2024), https://doi.org/10.1109/EPEPS61853.2024.10754476.

22. D. M. Pozar, *Microwave Engineering*, Fourth ed. (Wiley, 2011).

23. E. Matt Commens, Ansys Inc., "*Theres No Such Thing as Ground (But Perhaps Theres a Bob) Minimze Your Ports*," (2021).

24. W. Sun, "Accurate EM Simulation of SMT Components in RF Designs," in *2017 IEEE Radio Frequency Integrated Circuits Symposium (RFIC)* (IEEE, 2017), https://doi.org/10.1109/RFIC.2017.7969037.